

Plasmon-enhanced upconversion fluorescence in NaYF₄:Yb/Er/Gd nanorods coated with Au nanoparticles or nanoshells

Z. Q. Li, S. Chen, J. J. Li, Q. Q. Liu, Z. Sun et al.

Citation: *J. Appl. Phys.* **111**, 014310 (2012); doi: 10.1063/1.3676258

View online: <http://dx.doi.org/10.1063/1.3676258>

View Table of Contents: <http://jap.aip.org/resource/1/JAPIAU/v111/i1>

Published by the [American Institute of Physics](#).

Related Articles

Optical anisotropy of GaSb type-II nanorods on vicinal (111)B GaAs
Appl. Phys. Lett. **99**, 231901 (2011)

Microcavity effects in SiGe/Si heterogeneous nanostructures prepared by electrochemical anodization of SiGe/Si multiple quantum wells
J. Appl. Phys. **110**, 103101 (2011)

Tailoring the Faraday effect by birefringence of two dimensional plasmonic nanorod array
Appl. Phys. Lett. **99**, 191107 (2011)

Scattering analysis of plasmonic nanorod antennas: A novel numerically efficient computational scheme utilizing macro basis functions
J. Appl. Phys. **109**, 123109 (2011)

Tunable photoluminescence and photoconductivity in ZnO one-dimensional nanostructures with a second below-gap beam
J. Appl. Phys. **109**, 103523 (2011)

Additional information on J. Appl. Phys.

Journal Homepage: <http://jap.aip.org/>

Journal Information: http://jap.aip.org/about/about_the_journal

Top downloads: http://jap.aip.org/features/most_downloaded

Information for Authors: <http://jap.aip.org/authors>

ADVERTISEMENT

**AIP**Advances

Submit Now

**Explore AIP's new
open-access journal**

- **Article-level metrics
now available**
- **Join the conversation!
Rate & comment on articles**

Plasmon-enhanced upconversion fluorescence in NaYF₄:Yb/Er/Gd nanorods coated with Au nanoparticles or nanoshells

Z. Q. Li,¹ S. Chen,¹ J. J. Li,¹ Q. Q. Liu,¹ Z. Sun,¹ Z. B. Wang,² and S. M. Huang^{1,a)}

¹Engineering Research Center for Nanophotonics and Advanced Instrument, Ministry of Education, Department of Physics, East China Normal University, North Zhongshan Rd. 3663, Shanghai 200062, People's Republic of China

²Laser Processing Research Centre, School of Mechanical, Aerospace and Civil Engineering, University of Manchester, Sackville Street, Manchester, M60 1QD, United Kingdom

(Received 3 August 2011; accepted 14 December 2011; published online 12 January 2012)

We investigate plasmon-enhanced upconversion (UC) fluorescence in Yb³⁺-Er³⁺-Gd³⁺ codoped sodium yttrium fluoride (NaYF₄:Yb/Er/Gd) nanorods using gold nanoparticles or nanoshells. A simple method was proposed for the preparation of core/shell NaYF₄/Au structures, with dispersed Au nanoparticles or uniform Au coating on the surface of the UC nanorod. Pure hexagonal-phase NaYF₄:Yb/Er/Gd nanorods were synthesized via a liquid-solid reaction in oleic acid and ethanol solvent. A one-step approach was introduced to modify the hydrophobic surfaces of the as-deposited NaYF₄:Yb/Er/Gd nanorods. After this surface modification, Au nanoparticles or nanoshells were successfully attached on the surfaces of NaYF₄:Yb/Er/Gd nanorods. The as-deposited UC nanorods showed a strong UC emission in green and red bands under 980 nm laser excitation. The attachment of Au nanoparticles onto NaYF₄:Yb/Er/Gd nanorods resulted in a more than three-fold increase in UC emissions, whereas the formation of continuous and compact Au shells around the nanorods suppressed the emissions. The related interaction mechanisms of the UC emission of NaYF₄:Yb/Er/Gd nanorods with plasmon modes in Au nanostructures are analyzed and discussed. © 2012 American Institute of Physics. [doi:10.1063/1.3676258]

I. INTRODUCTION

The optical properties of nanoparticle structures have attracted great interest in recent years due to application-driven perspectives for the controllable manipulation of optical fields on micro- and nanoscale levels. The combination of localized surface plasmon resonances (SPRs) of individual metal particles and various particle structure configurations opens pathways for the realization of important effects such as strong-field confinement and enhancement,¹⁻⁵ light energy guiding along nanoparticle chains,⁶ surface-enhanced Raman spectroscopy with sensitivity down to a single molecule,⁷ and surface enhanced fluorescence (SEF) from nearby molecules.⁸ The first experimental and theoretical reports on SEF date back to the 1970s and 1980s,⁹ but such enhancements have been overshadowed by the much larger ones (with factors of 10⁵ to 10¹⁰) seen with surface-enhanced Raman scattering.¹⁰ SEF occurs primarily as a result of the interactions between the excited state of a fluorophore with the near-fields of an excited metal nanostructure, increasing the optical excitation rate and altering both radiative and nonradiative decay rates for the molecule. In the past decade, SEF has been widely reported with dyes and quantum dots.¹¹⁻¹³ Recently, new upconversion (UC) nanomaterials have drawn much attention. New synthesis routines offered ways to form lanthanide-doped nanometer-sized crystals in order to share the high efficiencies of their bulk equivalents.^{14,15} UC nanomaterials, however, usually have low emission efficiency

due to their structural defects and large surface areas with a variety of quenchers. Prior studies suggested that an enhanced UC efficiency could be obtained by using plasmonic interactions between UC nanocrystals and gold nanostructures. Schietinger *et al.* observed a great UC emission enhancement from single Yb³⁺-Er³⁺ codoped sodium yttrium fluoride (NaYF₄:Yb³⁺/Er³⁺) nanocrystal coupled with gold spheres via the use of an atomic force microscope.¹⁴ Zhang *et al.* reported an enhanced UC emission of hexagonal NaYF₄:Yb³⁺/Tm³⁺ nanocrystals coupled with gold nanoparticles or nanoshells.¹⁶ But to date, the maximum enhancement available in fluorescence has not been established. Moreover, the role of the plasmon resonance energy with respect to the excitation and emission energies of a fluorophore is not well understood. Studying the interactions of metal nanostructures with nanosized emitters is a strong starting point for the development of SPR-based lighting devices, including solar cells and various nano-biological and nanoscale optical devices.

In this work, we investigate plasmon-enhanced UC in Yb³⁺-Er³⁺-Gd³⁺ codoped sodium yttrium fluoride (NaYF₄:Yb/Er/Gd) nanorods coated with Au nanoparticles or nanoshells under illumination with a 980 nm diode laser. A simple approach is proposed for preparing NaYF₄:Yb³⁺/Er³⁺/Gd³⁺ nanorods with core-shell structures using gold nanoparticles or nanoshells. Pure hexagonal-phase NaYF₄:Yb/Er/Gd nanorods were synthesized via a liquid-solid reaction in oleic acid and ethanol solvents.¹⁵ Gd³⁺ dopant ions played key roles in the formation of pure hexagonal phases of NaYF₄. We introduced a one-step approach to modify the hydrophobic surfaces of the as-deposited NaYF₄:Yb/Er/Gd nanorods.

^{a)}Author to whom correspondence should be addressed. Electronic mail: enp5591@yahoo.com.

Nonylphenol ethoxylate NP-10 was used as an amphiphilic surfactant to modify the nanorod surfaces. After this surface modification, gold nanoparticles or nanoshells were successfully attached on the surfaces of NaYF₄:Yb/Er/Gd nanorods to form core-shell structured nanorods. It is found that the UC fluorescence of NaYF₄:Yb/Er/Gd nanorods coupled with Au nanoparticles increases more than three-fold. The related interaction and coupling mechanisms of UC emissions of NaYF₄:Yb/Er/Gd nanorods with plasmon modes in Au nanostructures are analyzed and discussed.

II. EXPERIMENTAL

A. Synthesis of NaYF₄:Yb/Er/Gd (18/2/30 mol. %) nanorods

NaYF₄:Yb/Er/Gd nanorods were grown according to the procedures described in Ref. 15. A de-ionized (DI) water solution (7.5 ml) of 1.5 g NaOH was mixed with 25 ml of ethanol and 25 ml of oleic acid under stirring. Ten ml of RECl₃ (0.2 M) (RE = Y, Yb, Er, and Gd, YCl₃:YbCl₃:ErCl₃:GdCl₃ = 50:18:2:30 mol. %) solution and 5 ml of NH₄F (2 M) was added to the resulting mixture. Then, the solution was transferred into a 100 ml Teflon-lined autoclave and heated at 200 °C for 2 h to obtain the nanorods. The nanorods were washed with ethanol and water several times and collected via centrifugation. Finally, the nanorods were re-dispersed into water to form an aqueous dispersion and were ready for use.

B. Attachment of gold nanoparticles

A gold nanoseed solution was prepared by a modified procedure presented in Refs. 16–18. Twenty-four μl of 80% tetrakis (hydroxymethyl) phosphonium chloride and 0.5 ml of 2 M NaOH were added to 90 ml of DI water. The mixture was stirred vigorously for at least 15 min. Then, 4 ml of 1 wt. % HAuCl₄ was quickly added to the resulting mixture. The color of the solution changed rapidly from colorless to dark brown. The resulting gold nanoseed solution was stored in a lightproof container with stirring overnight. One ml of nonylphenol ethoxylate NP-10, 1 ml of 0.01 M NaYF₄:Yb/Er/Gd nanorod solution in cyclohexane, 5 ml of cyclohexane, and 10 ml of Au nanoseed solution were mixed and stirred vigorously at room temperature for 1 to 24 h.

C. Growth of gold nanoshells

An aged gold solution was prepared using a modified procedure from Refs. 16–18. A solution was prepared by dissolving 0.05 g of potassium carbonate in 200 ml of DI water and stirring for 15 min. Then, 4 ml of 1 wt. % HAuCl₄ was added to the solution. The solution turned colorless after approximately 10 min. The resulting solution was aged by storing it in the refrigerator for at least 1 day. One ml of UC nanorod solution (with gold nanoseeds attached) was added to 10 ml of the aged gold solution with stirring. After stirring, 0.02 ml of formaldehyde and 0.05 ml of ammonium hydroxide were introduced simultaneously. Upon mixing, the color of the mixture immediately changed from colorless to brownish-blue, and a black precipitate was obtained quickly.

D. Characterization and photoelectron measurements

NaYF₄:Yb³⁺/Er³⁺/Gd³⁺ nanorods before and after Au nanoparticle attachment or nanoshell growth were examined and characterized. The transmission electron microscopy (TEM) images were recorded on a JEOL 2010 F transmission electron microscope. Fluorescence spectra were recorded on a HORIBA Jobin Yvon fluoromax-4 fluorescence spectrophotometer equipped with a commercial near-infrared laser (980 nm). Ultraviolet and visible (UV-Vis) spectra were acquired with a Hitachi U-3900 UV-Vis spectrophotometer, and the Fourier transform infrared (FTIR) spectra were taken using a Nicolet 6700 spectrometer.

III. RESULTS AND DISCUSSION

The controlled synthesis of gold nanoparticles or nanoshells is usually carried out in aqueous solution, requiring the dispersion of UC nanorods in water. However, NaYF₄:Yb/Er/Gd nanorods synthesized via the liquid-solid reaction in oleic acid and ethanol solvents are terminated with oleic acid ligands, which are hydrophobic. Various methods have been reported for modifying UC material surfaces. Yang *et al.* employed Triton X-100 to modify the hydrophobic property of the UC nanocrystal surface.¹⁹ Li *et al.* reported a surface modification process with the help of CO-520.²⁰ Recently, Zhang *et al.* reported a two-step method for displacing the original hydrophobic ligands on the surfaces of NaYF₄:Yb/Tm hexaplate nanocrystals using polyacrylic acid and polyallylamine hydrochloride (successively), resulting in UC nanocrystals with high water dispersibility.¹⁶ In this work, we proposed an alternative one-step approach for modifying UC nanorod surfaces. Nonylphenol ethoxylate NP-10 was used as an amphiphilic surfactant to modify the hydrophobic surface of the NaYF₄:Yb/Er/Gd nanorods. The hydrophobic segment of nonylphenol ethoxylate NP-10 interacted with the alkyl chain of oleic acid on the outside surfaces of the nanorods, rendering hydrophilic ligands dispersed on the surfaces of UC nanorods. As a result, after this surface modification, gold nanoparticles or nanoshells can be attached on the surfaces of NaYF₄:Yb/Er/Gd nanorods. FTIR analysis was examined in order to confirm the successful surface modification of UC nanorods. Figure 1 shows the FTIR spectra of NaYF₄:Yb/Er/

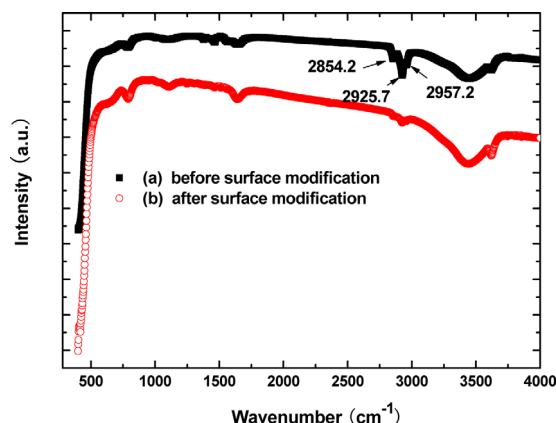


FIG. 1. (Color online) FTIR spectra of NaYF₄:Yb/Er/Gd nanorods before and after surface modification.

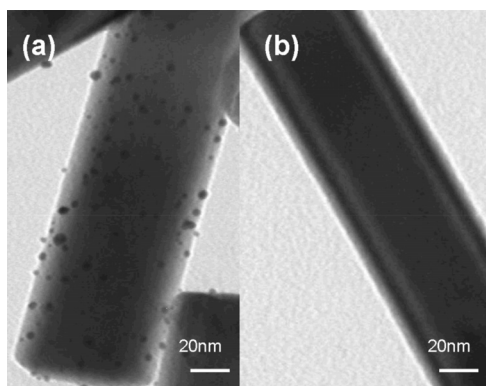


FIG. 2. TEM images of (a) NaYF₄:Yb/Er/Gd nanorod with Au nanoparticles and (b) NaYF₄:Yb/Er/Gd nanorod with Au shell.

Gd nanorods before and after the surface modification. In Fig. 1(a), the FTIR spectrum of the as-synthesized nanorods contains strong -CH₃ bands centered at 2854.2, 2925.7, and 2957.2 cm⁻¹. In Fig. 1(b), these three bands almost disappear, suggesting that our method successfully modified the surface property of the NaYF₄:Yb/Er/Gd nanorods.

The microstructures and morphologies of NaYF₄:Yb/Er/Gd nanorods without or with Au nanostructures were characterized via TEM. The as-prepared UC nanorods have a hexagonal structure with a uniform size of 70 to 80 nm in diameter and approximately 300 to 500 nm in length. These results are consistent with those of NaYF₄:Yb/Er/Gd (18/2/30 mol. %) samples reported in Ref. 15. Figure 2 shows TEM images of NaYF₄:Yb/Er/Gd nanorods with attached gold nanoparticles 24 h after the Au attachment process and with gold shells after 10 min of the Au shell reaction. It was found that during the addition of gold nanoparticles, the number of dark specks in Fig. 2(a) increased with increasing process time. Each dark speck corresponded to a gold nanoparticle (4 to 8 nm in size) on the nanorod surface. These Au nanoparticles functioned as nucleation centers for the growth of a shell. As the shell reaction proceeded, these nanoseeds grew rather quickly and eventually merged together to form a continuous Au shell around the nanorod, as shown in Fig. 2(b).

Figure 3 shows the UV-Vis absorption spectra of UC nanorods during the gold seed attachment (0-24 h) and shell formation (0-10 min) stages. The spectra of these nanorods (ca. 1 wt. %) were collected in an ethanol solution. For UC nanorods with Au nanoparticles formed at different times, there is a small peak at about 310 nm but no absorption peak in the visible light or near-infrared (NIR) regions. In contrast, the spectra of nanorods covered with Au shells formed at 5 and 10 min, respectively, show a peak around 530 nm in Fig. 3(b).

Figures 4(a) and 4(b) show UC emission spectra of NaYF₄:Yb/Er/Gd nanorods during the gold nanoparticle attachment (0-24 h) and gold shell formation (0-10 min) stages, respectively. The emission spectra were collected under 980 nm laser excitation with a power of 500 mW at room temperature. For the as-synthesized NaYF₄:Yb/Er/Gd nanorods, the spectrum exhibits two strong emission bands at 540 and 660 nm and a weak emission peak at 524 nm, corresponding to ⁴S_{3/2} → ⁴I_{15/2}, ⁴F_{9/2} → ⁴I_{15/2}, and ²H_{11/2} → ⁴I_{15/2} transi-

tions of Er³⁺, respectively.^{14,21} The emission spectrum of the UC nanorods during the Au nano-seeding stage shows a significant increase in emission intensity as the seeding duration increases and the number of attached Au nanoparticles rises, as shown in Fig. 4(a). Additionally, the emission enhancement by Au nanoparticles is wavelength-dependent, as the enhancement factors in the green region (540 nm) are a little less than those in the red region (660 nm). Compared with the case of the as-synthesized NaYF₄:Yb/Er/Gd nanorods without Au nanostructures, the green emission intensity of UC nanorods with Au nanoparticles increases by a factor of 3.8, and the red emission intensity has an enhancement factor of 4.0 after a 24 h gold seed attachment stage. Furthermore, fluorescence quenching was observed during the gold shell formation stage in Fig. 4(b). Compared with the case of NaYF₄:Yb/Er/Gd nanorods after the 24 h Au nanoparticle attachment, a decrease in the green emission was observed with increasing Au shell formation time, whereas an increase in the red spectral emission was noticed at the initial Au shell formation stage from 0 to 10 min. With a further increase in the shell formation time from 10 min, the emission intensity was found to decrease substantially at both green and red bands. These results demonstrate that the attachment of Au nanoparticles on the UC nanorod surfaces can enhance the UC emission, whereas the evolution of continuous and compact Au shells around the UC nanorod cores can quench both green and red emissions.

Time-resolved spectra and UC luminescence lifetimes were measured for NaYF₄:Yb/Er/Gd nanorods without and

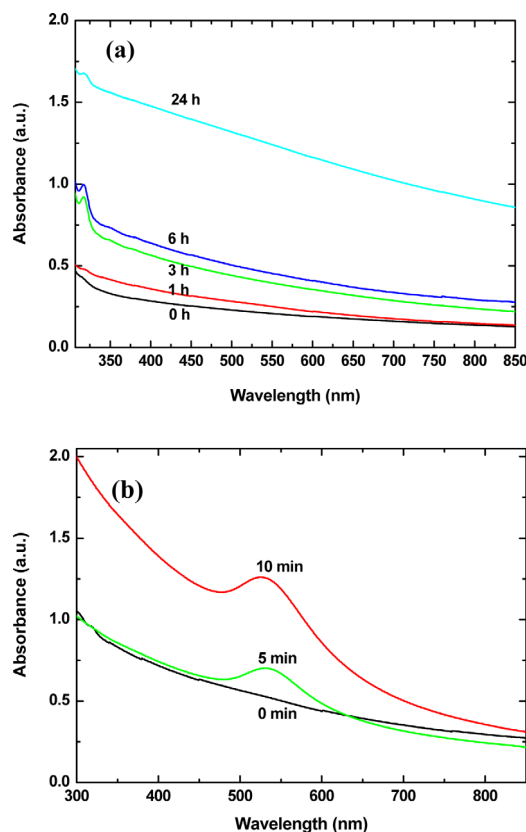


FIG. 3. (Color online) UV-Vis spectra of NaYF₄:Yb/Er/Gd nanorods during Au nanostructure process: (a) gold nanoparticle attachment stage (0-24 h), (b) gold shell formation stage (0-10 min).

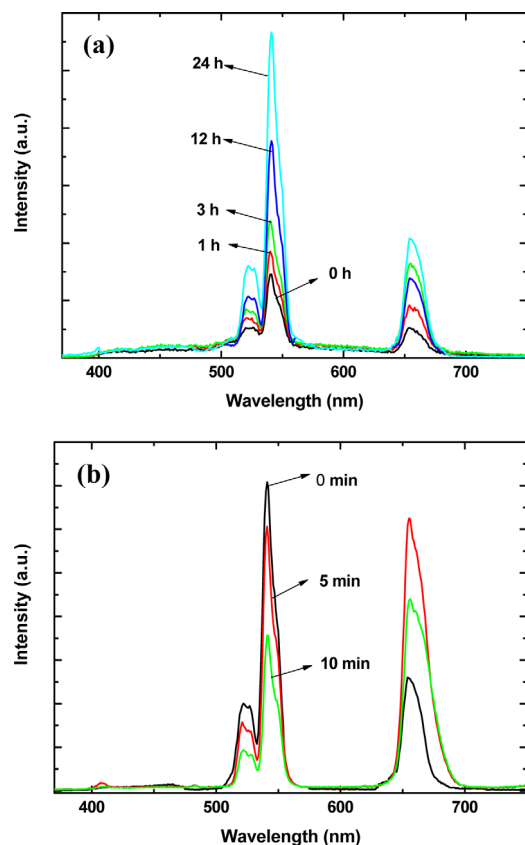


FIG. 4. (Color online) Upconversion emission spectra of $\text{NaYF}_4:\text{Yb}/\text{Er}/\text{Gd}$ nanorods during (a) gold nanoparticle attachment stage (0-24 h) and (b) gold shell formation stage (0-10 min).

with Au nanostructures under 980 nm laser excitation using a customized phosphorescence lifetime spectrometer equipped with a digital oscilloscope. As neither the rise nor the decay time of the fluorescence is monoexponential, we determine the time (τ) for the signal to rise (decay) to half of its maximal value. The rise and decay times of the green and red UC emissions from bare UC nanorods and nanorods with Au nanostructures (particles at a duration time of 24 h and shells

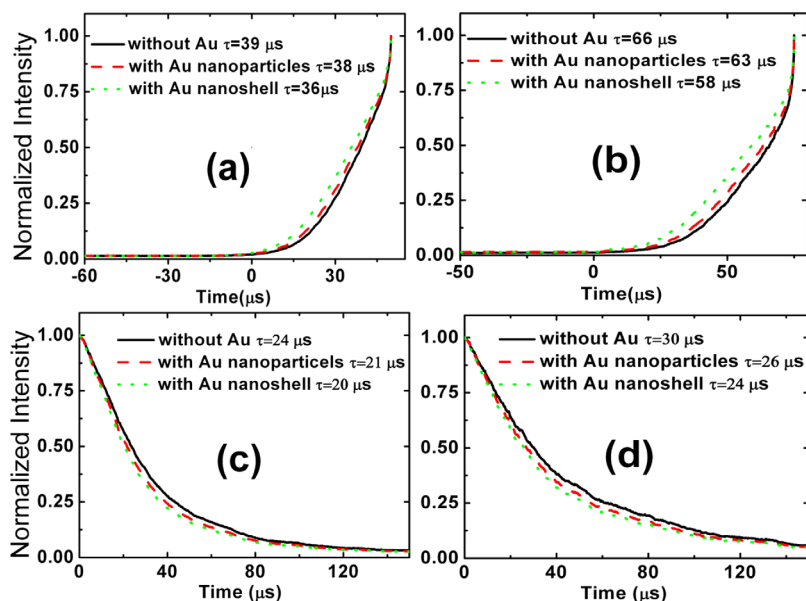


FIG. 5. (Color online) Rise and decay times for $\text{NaYF}_4:\text{Yb}/\text{Er}/\text{Gd}$ nanorod without and with Au nanostructures (particles at duration time of 24 h and shells at duration time of 5 min): (a) rise time at 540 nm, (b) rise time at 660 nm, (c) decay time at 540 nm, and (d) decay time at 660 nm.

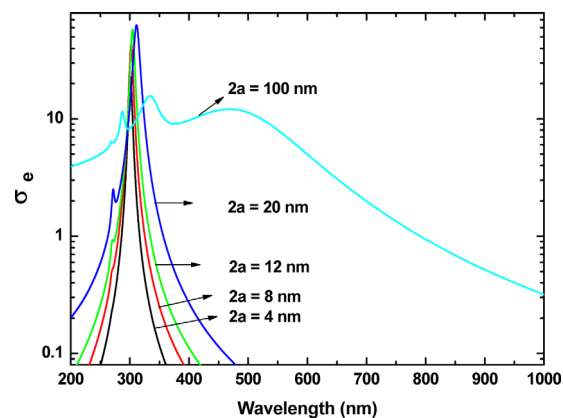


FIG. 6. (Color online) Calculated extinction cross sections (σ_e) of Au spheres (radius a) of different sizes (4 to 100 nm).

at a duration time of 5 min) are shown in Figs. 5(a)–5(d). The evolution of the green UC emission from bare UC nanorods was with a rise time of $\tau = 39 \mu\text{s}$ and a decay time of $\tau = 24 \mu\text{s}$, whereas the red emission from bare nanorods presented a rise time of $66 \mu\text{s}$ and a decay time of $30 \mu\text{s}$. Both the rise and the decay times were reduced after coupling of UC nanorods with Au nanoparticles or Au nanoshells.

As is well known, SPRs of individual metal particles and various particle structure configurations offer ways for the realization of strong-field confinement and enhancement.^{1–5} The optical response, SPRs, and local field distributions are strongly dependent on the particle shape, size, and distribution; the interaction between particles; and the polarization of the incident light.^{2–5,22,23} Fig. 6 shows the computed extinction cross sections (σ_e) of Au spheres with different diameters (4 to 100 nm) based on the extended Mie theory reported by Ruppin.²² The dielectric constant (ϵ_M) of the medium surrounding the sphere (ethanol) is 1.36.² As the size of the sphere is increased from 4 to 20 nm, the main longitudinal plasmon resonance displays a slight red-shift from 301 to 309 nm. When the size of the sphere increases up to 100 nm, the image in Fig. 6 shows an extinction maximum at 320 nm together with another broad band that exhibits a strong σ_e

value from the NIR through the visible to the ultraviolet range. Au nanoparticles even after 24 h of the seeding process are sparsely distributed on the surfaces of the UC nanorods, and the particle size is about 4 to 8 nm, as shown in Fig. 2(a). Thus, the calculation results based on a single sphere (radius a) model shown in Fig. 6 can well explain the optical properties of UC nanorods with Au nanoparticles. The small bands at about 310 nm in the absorption spectra shown in Fig. 3(a) could correspond to the longitudinal plasmon resonance of the Au nanoseeds. In the Au nanoshell geometry, the plasmon resonance frequency is a sensitive function of the relative dimensions of the core and shell and can be shifted hundreds of nanometers in wavelength from the plasmon resonance of the corresponding Au nanoparticle.²⁴ As a result, when those Au nanoseeds were transformed into continuous shells, the resonant peak red-shifted to 530 nm, as shown in Fig. 3(b).

For simple spheres, a separation of variables approach²⁵ allows calculation of the field intensity both internal and external to the sphere. For the dielectric functions we consider the size effect of the surface scattering of the sphere. Au nanoparticles absorb energy through both the collective excitation of free electrons and the electron transition of bound electrons from occupied to empty bulk band (called inter-band transitions).²⁶ Therefore, the dielectric function of gold, by considering the size effect of the surface scattering, can be written as

$$\varepsilon = \varepsilon_{inter} + 1 - \frac{\omega_p^2}{\omega^2 + i\omega(\gamma_{bulk} + \gamma_{sur})}, \quad (1)$$

where ω_p is the bulk plasma frequency of gold, γ_{bulk} is the damping constant in the bulk, $\gamma_{sur} = A(v_F/a)$ represents the surface scattering term, A is a constant [for a sphere, $A = 1$ (Ref. 27)], and v_F is the Fermi velocity of the electron cloud. Surface scattering contributes to the broadening of the resonant peak but does not shift the localized surface plasmon resonance wavelength.²⁶ In the present study, the value of the parameters $v_F = 1.4 \times 10^6 \text{ ms}^{-1}$, $\omega_{inter} = 8.9$, $\omega_p = 1.36 \times 10^{16} \text{ s}^{-1}$, and $\tau_{bulk} = 1/\gamma_{bulk} = 9.1 \times 10^{-15} \text{ s}$ are considered from the literature.²⁸ In the small-particle approximation ($q = 2\pi a/\lambda \ll 1$),²⁵ we consider the amplitude of the electric vector of the incident plane wave as normalized to unity; the wave propagates along the z -coordinate, the electric vector is directed along the x -coordinate, and the magnetic vector is along the y -coordinate. In the spherical coordinate system with the origin situated at the sphere's center, the incident, scattered, and internal electric fields for parallel polarization can be expressed as

$$E^i = E_0 \mathbf{i}_x = E_0 [\sin \theta \cos \varphi \mathbf{i}_r + \cos \theta \cos \varphi \mathbf{i}_\theta - \sin \varphi \mathbf{i}_\varphi], \quad (2)$$

$$E^s = E_0 \frac{\varepsilon - 1}{\varepsilon + 2} \left(\frac{a}{r}\right)^3 [2 \sin \theta \cos \varphi \mathbf{i}_r - \cos \theta \cos \varphi \mathbf{i}_\theta + \sin \varphi \mathbf{i}_\varphi], \quad (3)$$

$$E^{int} = E_0 \frac{3}{\varepsilon + 2} \left(\frac{a}{r}\right)^3 [\sin \theta \cos \varphi \mathbf{i}_r + \cos \theta \cos \varphi \mathbf{i}_\theta - \sin \varphi \mathbf{i}_\varphi]. \quad (4)$$

Because the term in the brackets in Eq. (4) is the unit vector \mathbf{i}_x , the internal electric field is constant and in the same direction as the incident field. The total external electric field is given by the sum of Eqs. (2) and (3).

$$E^{ext} = E_0 \left[\frac{2(\varepsilon - 1)}{\varepsilon + 2} \left(\frac{a}{r}\right)^3 + 1 \right] \sin \theta \cos \varphi \mathbf{i}_r - E_0 \left[\frac{\varepsilon - 1}{\varepsilon + 2} \left(\frac{a}{r}\right)^3 - 1 \right] (\cos \theta \cos \varphi \mathbf{i}_\theta - \sin \varphi \mathbf{i}_\varphi). \quad (5)$$

Because of the symmetry of the sphere, the angle-averaged intensity is independent of the incident polarization. The calculated quantity is

$$I_{avg}(r) = \frac{1}{4\pi} \int_0^{2\pi} \int_0^\pi \mathbf{E} \cdot \mathbf{E}^* \sin \theta d\theta d\varphi, \quad (6)$$

where \mathbf{E} is either the internal electric field or the total external (the sum of the incident and scattered) electric field. From Eq. (5), the distribution of the total external intensity in the xy plane at $z = a$ for the Au sphere ($a = 4 \text{ nm}$), illuminated by radiation with $\lambda = 980 \text{ nm}$ and parallel polarization, is shown in Fig. 7. For a Au nanoparticle, there are electrical field enhancements in regions around the sphere but not directly under the sphere, as shown in Fig. 7(a). The

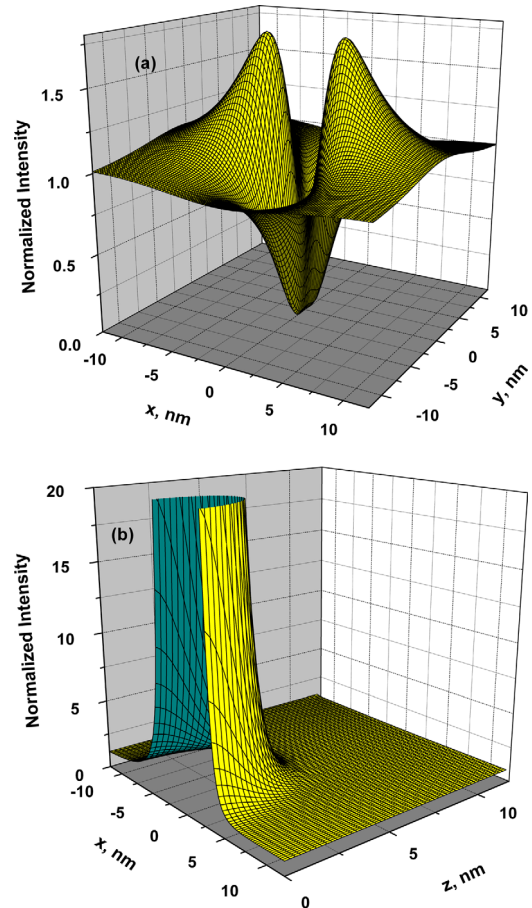


FIG. 7. (Color online) Total external intensity distribution for a Au sphere ($a = 4 \text{ nm}$) illuminated by radiation with $\lambda = 980 \text{ nm}$ and parallel polarization. (a) 3D picture of the intensity distribution in the xy plane at $z = a$. (b) 3D picture of the intensity distribution in the xz plane at $y = 0$.

maximum intensity enhancement in calculations is about 1.7 in the xy plane. However, the total external intensity in the region around the sphere in the xz plane at $y = 0$ is far more intense, as shown in Fig. 7(b). From Eq. (6), the angle-averaged intensity enhancement at $r = a$ is 2.99. With other radiation wavelengths such as 540 nm and 650 nm, the total external intensity distribution will change a little, but with contour results similar to the one in Fig. 7. The angle-averaged intensity enhancement at $r = a$ is 2.71 and 2.93 for 540 nm and 650 nm radiations, respectively.

The observed enhancement in the UC emission with the presence of gold nanoparticles shown in Fig. 4(a) can be due to at least two effects. An enhanced effective excitation flux results in an increase of the excitation rate. The enhanced excitation flux is caused by local field enhancement associated with plasmonic resonance, as shown in Fig. 7. We think that it is the “hot regions” around Au spheres in which high electrical field, and thus enhancement of UC emission, occurs, as shown in Fig. 4(a). The angle-averaged intensity enhancement of 2.99 at $r = a$ is very close to the UC emission enhancement value of UC nanorods coupled with gold nanoparticles under the irradiation of a 980 nm laser. On the other side, the emission rate was further increased due to surface plasmon-coupled emission because of the coupling of the UC emission with the nanostructure plasmonic resonance. This coupling can occur when the emission band of the fluorophore overlaps with the plasmon resonance frequency of the metal nanostructures.²⁹ The Er emission green ($^4S_{3/2} \rightarrow ^4I_{15/2}$) and red ($^4F_{9/2} \rightarrow ^4I_{15/2}$) bands are centered at around 540 nm and 660 nm, respectively.³⁰ For a Au sphere illuminated by radiation with $\lambda = 540$ nm or $\lambda = 660$ nm, the total external intensity distributions also show hot regions similar to those in Fig. 7, corresponding to the dipolar resonances. Au nanoparticles support these dipolar modes that are resonant with the Er emission, resulting in an increase of the excitation rate and enhancement of the UC emission. Under illumination by radiation with $\lambda = 540$ nm and $\lambda = 660$ nm, the angle-averaged intensity enhancement is 2.71 and 2.93, respectively. The slightly higher red emission enhancement factor of nanorods with Au nanoparticles shown in Fig. 4(a) can be attributed to the higher averaged intensity enhancement at the wavelength of 660 nm. The plasmonic enhancement effect on the emission of UC nanorods in the presence of Au nanoparticles is also reflected in a reduction of the rise and decay times in Fig. 5.

With the formation of gold shells from Au seeds on UC nanorods, the rise and decay times were further decreased (Fig. 5), and a quench was observed as shown in Fig. 4(b). The formation of the continuous and compact gold shell quenched both green and red emissions. The spectra of nanorods covered with Au shells formed at 5 and 10 min show a peak around 530 nm in the absorption spectrum shown in Fig. 3(b). Thus, the SPR band for UC nanorods coated with Au nanoshells is at around 530 nm. As the plasmon resonance around 530 nm overlaps more strongly with the green emission band compared to the case of the nanorod-Au nanoparticle complex, one would indeed expect a stronger enhancement in the green emission process. However, the excitation field and the emitted radiation can be enhanced,

but quenching by energy transfer and nonradiative relaxation in metal is also possible.^{14,16} In our work, the quenching can be explained by the following consideration. In the configuration of UC nanorod-Au nanoparticles, excitation and emission were enhanced, and the Au nanoparticles were distributed too sparsely to introduce quenching of the emission. But in the case of a Au shell completely surrounding the UC nanorod, additional quenching competed with any further amplification of the fluorescence. Moreover, the compact gold shell might block the emission transmittance from the UC nanorods, leading to the quenching of the UC emission at both green and red bands as shown in Fig. 4(b). The overall UC emission intensity is influenced by the excitation rate, emission rate, and quenching effect. As shown in Fig. 5, both the excitation rate and the decay rate are wavelength-dependent; as a result, the enhancement or quenching of the emission intensity is different at 540 nm and at 660 nm.

The grown NaYF₄:Yb/Er/Gd nanorods without or with Au nanoparticles offered strong UC emissions in both green and red bands under the NIR light. Therefore, they can be expected to be applied in solar cell technologies and to allow an increase in the efficiency of the photo-conversion process in the infrared-region, a range that is notoriously poor for the current commercial solar cells. We initially examined the feasibility of using the prepared UC nanorods in solar cells and fabricated dye-sensitized solar cells (DSSCs) by modifying the device synthesis procedures reported in our previous work^{31,32} and by coating NaYF₄:Yb³⁺/Er³⁺/Gd³⁺ nanorods on N719 dye-sensitized TiO₂ films. Under the illumination of the 980 nm laser, the DSSC without using UC nanorods showed a short-circuit current (I_{SC}) of 0.317 mA and an open-circuit voltage (V_{OC}) of 0.672 V, whereas the cell coated with UC nanorods displayed a I_{SC} of 0.368 mA and a V_{OC} of 0.695 V. Our preliminary work showed that the performance of the DSSC was obviously improved with UC nanorods because the NIR light was converted *in situ* to dye-absorbable visible light. More experimental and theoretical work is being carried out. Furthermore, these UC nanorods also have high transmission in the visible wavelength range, and the prepared UC materials can be employed and added to any solar cell technology—crystalline, thin-film, and organic/hybrid solar cells. The grown UC nanorods can be applied to the back side or the front side of a solar cell to improve its infrared response. Therefore, the prepared UC nanorods and nanomaterials in combination with metal nanostructures have great potential to be used in the energy system of photovoltaic cells, as well as in nano-biological devices.

IV. CONCLUSIONS

The plasmon-enhanced UC fluorescence in Yb³⁺-Er³⁺-Gd³⁺ codoped sodium yttrium fluoride (NaYF₄:Yb/Er/Gd) nanorods has been investigated. The as-deposited UC nanorods showed intense UC emission in green and red regions under excitation with a 980 nm laser. When UC nanorods were coupled with gold nanoparticles, the UC emission intensity at 540 nm increased by a factor of 3.8, and the emission intensity at 660 nm had an enhancement factor of 4.0. When nanorods were surrounded by continuous and compact Au

shells, UC emissions were suppressed. Theoretical small-particle approximation calculations support the experimental plasmon-enhanced UC results of NaYF₄:Yb/Er/Gd nanorods in combination with gold nanoparticles. The unique properties and functions offered by UC NaYF₄:Yb/Er/Gd nanorods will enable its wide implementation in photovoltaic applications.

ACKNOWLEDGMENTS

This work was supported by the National Natural Science Foundation of China (Grant No. 10774046) and Shanghai Municipal Science & Technology Commission Funds (Grant No. 09JC1404600).

- ¹Z. B. Wang, B. S. Luk'yanchuk, M. H. Hong, Y. Lin, and T. C. Chong, *Phys. Rev. B* **70**, 035418 (2004).
- ²Z. Wang, W. Guo, L. Li, B. Luk'yanchuk, A. Khan, Z. Liu, Z. Chen, and M. Hong, *Nature Communications* **2**, 218 (2011).
- ³S. M. Huang, B. S. Luk'yanchuk, M. H. Hong, and T. C. Chong, *Appl. Phys. Lett.* **82**, 4809 (2003).
- ⁴S. M. Huang, Z. Sun, B. S. Luk'yanchuk, M. H. Hong, and L. P. Shi, *Appl. Phys. Lett.* **86**, 161911 (2005).
- ⁵P. Mühlischlegel, H.-J. Eisler, O. J. F. Martin, B. Hecht, and D. W. Pohl, *Science* **308**, 1607 (2005).
- ⁶S. A. Maier, P. G. Kik, H. A. Atwater, S. Meltzer, E. Harel, B. E. Koel, and A. A. G. Requicha, *Nature Mater.* **2**, 229 (2003).
- ⁷W. Zhang, X. Cui, B. S. Yeo, T. Schmid, C. Hafner, and R. Zenobi, *Nano Lett.* **7**, 1401 (2007).
- ⁸J. R. Lakowicz, *Anal. Biochem.* **298**, 1 (2001).
- ⁹K. H. Drexhage, in *Progress in Optics*, edited by E. Wolfe (North-Holland, Amsterdam, 1974).
- ¹⁰*Surface-Enhanced Raman Scattering: Physics and Applications: Topics in Applied Physics*, edited by K. Kneipp, M. Moskovits, and H. Kneipp (Springer, Berlin, 2006).
- ¹¹H. Diltbacher, J. R. Krenn, N. Felidj, B. Lamprecht, G. Schider, M. Salerno, A. Leitner, and F. R. Aussenegg, *Appl. Phys. Lett.* **80**, 404 (2002).
- ¹²J. S. Biteen, N. S. Lewis, H. A. Atwater, H. Mertens, and A. Polman, *Appl. Phys. Lett.* **88**, 131109 (2006).
- ¹³J. A. Schuller, E. S. Barnard, W. Cai, Y. C. Jun, J. S. White, and M. L. Brongersma, *Nature Mater.* **9**, 193 (2010).
- ¹⁴S. Schietinger, T. Aichele, H. Q. Wang, T. Nann, and O. Benson, *Nano Lett.* **10**, 134 (2010).
- ¹⁵F. Wang, Y. Han, C. S. Lim, Y. Lu, J. Wang, J. Xu, H. Chen, C. Zhang, M. Hong, and X. G. Liu, *Nature* **463**, 1061 (2010).
- ¹⁶H. Zhang, Y. J. Li, I. A. Ivanov, Y. Q. Qu, Y. Huang, and X. F. Duan, *Angew. Chem., Int. Ed.* **49**, 2865 (2010).
- ¹⁷S. L. Westcott, S. J. Oldenburg, T. R. Lee, and N. J. Halas, *Langmuir* **14**, 5396 (1998).
- ¹⁸J. H. Kim, W. W. Bryan, and T. R. Lee, *Langmuir* **24**, 11147 (2008).
- ¹⁹J. Yang, Y. Deng, Q. Wu, J. Zhou, H. Bao, Q. Li, F. Zhang, F. Li, B. Tu, and D. Zhao, *Langmuir* **26**, 8850 (2010).
- ²⁰Z. Li, Y. Zhang, and S. Jiang, *Adv. Mater.* **20**, 4765 (2008).
- ²¹F. Wang, J. Wang, and X. G. Liu, *Angew. Chem., Int. Ed.* **49**, 7456 (2010).
- ²²R. Ruppini, *Phys. Rev. B* **11**, 2871 (1975).
- ²³K. L. Kelly, E. Coronado, L. L. Zhao, and G. C. Schatz, *J. Phys. Chem. B* **107**, 668 (2003).
- ²⁴R. D. Averitt, D. Sarkar, and N. J. Halas, *Phys. Rev. Lett.* **78**, 4217 (1997).
- ²⁵P. W. Barber and S. C. Hill, *Light Scattering by Particles: Computational Methods* (World Scientific, Singapore, 1990), pp. 188–239.
- ²⁶C. Noguez, *J. Phys. Chem. C* **111**, 3806 (2007).
- ²⁷U. Kreibitz, *J. Phys. F: Met. Phys.* **4**, 999 (1974).
- ²⁸M. M. Alvarez, J. T. Khoury, T. G. Schaff, M. N. Shafiqullin, I. Vezmar, and R. L. Whetten, *J. Phys. Chem. B* **101**, 3706 (1997).
- ²⁹Y. Liu, D. Tu, H. Zhu, R. Li, W. Luo, and X. Chen, *Adv. Mater.* **22**, 3266 (2010).
- ³⁰A. S. Oliveira, M. T. de Araujo, A. S. Gouveia-Neto, J. A. Medeiros Neto, A. S. B. Sombra, and Y. Messaddeq, *Appl. Phys. Lett.* **72**, 753 (1998).
- ³¹X. D. Li, D. W. Zhang, S. Chen, Z. A. Wang, Z. Sun, X. J. Yin, and S. M. Huang, *Mater. Chem. Phys.* **124**, 179 (2010).
- ³²D. W. Zhang, X. D. Li, S. Chen, Z. Sun, X. J. Yin, and S. M. Huang, *Microchim. Acta* **174**, 73 (2011).